Supporting information

Au-Decorated $Zn_xMg_{1-x}O$ Solid Solutions with Coexisting Acidic and Basic Sites for Enhanced Photocatalytic Methane Conversion to Ethane

Xiaoyan Feng[a], Jun Liang[a,*], Ping Wang[a], Jinni Shen[b,*], Jinyu Zhang[a], Li Li[a,*]

[a]*State Key Laboratory of High-efficiency Utilization of Coal and Green Chemical Engineering, College of Chemistry and Chemical Engineering, Ningxia University, Yinchuan 750021, P. R. China.*

[b]*State Key Lab of Photocatalysis on Energy and Environment, College of Chemistry Fuzhou University, Fuzhou, 350116, P. R. China.*

[a]E-mail: junliang@nxu.edu.cn

[b]E-mail: t15067@fzu.edu.cn

[a]E-mail: li_l@nxu.edu.cn

*Corresponding authors.

1. EXPERIMENTAL SECTION

1.1 Characterization

The crystal structure and phase composition were assessed by Powder X-ray diffraction (XRD) (XRD, Rigaku Smart Lab 0303050201, Japan) with Cu Kα radiation at a scanning speed of 10°/min. The morphology of the samples was observed by transmission electron microscopy (TEM, FEI Tecnai G2 F20). A high-resolution TEM (HRTEM) was further used for microstructural analysis and the elemental distribution of samples. The ultraviolet visible diffuse reflectance spectrum (DRS) uses $BaSO_4$ as the reflectance standard to test the absorption band gap of the sample on a U-3010(Hitachi, Japan). X-ray photoelectron spectroscopy (XPS, Thermo Fisher ESCALABXI+, USA) was used to analyze the chemical state of the materials. The N_2 adsorption−desorption isotherm characterizations were conducted on Micromeritics ASAP 2020 under liquid nitrogen temperature (77 K). Temperature-programmed desorption (TPD) tests of CO_2 and CH_4 were performed by a chemisorber (Autochem II 2920). Electron paramagnetic resonance (EPR) spectra were recorded on MS-5000 electron spin paramagnetic resonance.

1.2 Photoelectrochemical measurements

The working electrode was made of a fluorine-doped tin oxide (FTO) glass sheet, which was ultrasonically cleaned in cleaning solution, acetone, and ethanol in sequence. Then, a certain amount of photocatalyst was dispersed in aqueous ethanol solution under the action of ultrasonic waves to form a suspension. The photocatalytic film was prepared by dispersing the suspension onto the conductive surface of the FTO glass. The photoelectrochemical test was performed in a typical three-electrode electrochemical cell on a CHI-77E workstation with an Ag/AgCl (saturated KCl solution) electrode as the reference electrode, a platinum foil as the counter electrode, and the catalyst-coated FTO glass electrode as the working electrode. Na_2SO_4 solution (0.2 M) was used as the electrolyte, and a 300 W xenon lamp was introduced as the light source. The electrochemical impedance spectroscopy (EIS) experiment was carried out in the mixed solution containing 0.5 M KCl and 5.0 mM $K_3[Fe(CN)_6]/K_4[Fe(CN)_6]$.

1.3 Calculation of Turnover frequency (TOF)

The calculation of TOF was based on the C_2 product yields over the active sites Au nanoparticle. Catalyst amount = 5 mg

Au molar amount = $\frac{Catalyst\ amount\ \times\ Au\ concentration}{The\ atomic\ weight\ of\ Au}$ = 0.76 μmol

TOF = $\frac{C_2\ yield\ rate \times 2}{Au\ molar\ amount}$ = 35.5 h^{-1}

Noted: The calculation was based on the active site, such as noble metal cocatalyst in their stability test periods. For those with more than one cocatalyst, the calculation was based on the sum of the co-catalysts amount used for CH_4 activation.

1.4 Calculation details

All structures were optimized using the Vienna Ab initio Simulation Package (VASP), implementing the GGA-PBE as the exchange-correlation functional[S-1, 2]. The projector augmented wave (PAW)[S-3] method was employed to manage the interactions between valence and core/inner electrons. The plane-wave basis set cutoff energy was established at 500 eV, while the convergence criteria for energy and force for all atoms were set to 10^{-6} eV and 0.05 eV·Å^{-1}, respectively. A k-point sampling of 1×1×1 centered at the Gamma point was employed within the Brillouin. To prevent interlayer interactions due to periodic boundary conditions, the vacuum layer thickness for the surface structures was set to 15 Å.

Based on experimental results, a ZnMgO solid solution model was created by substituting Mg for one Zn atoms in the wurtzite ZnO unit cell. From this model, a 4×6 ZnMgO(101) surface structure was developed. An Au_{13} cluster was subsequently added to the ZnMgO(101) surface to create the Au-ZnMgO model. The adsorption energy of the molecule on the surface is defined as

$$\Delta E = E_{*ads} - E_{ads} - E_{*}$$

where E_{*ads} is the total energy of the adsorbate-surface, E_{ads} is the energy of the isolated adsorbate, and E_{*} is the energy of the clean surface.

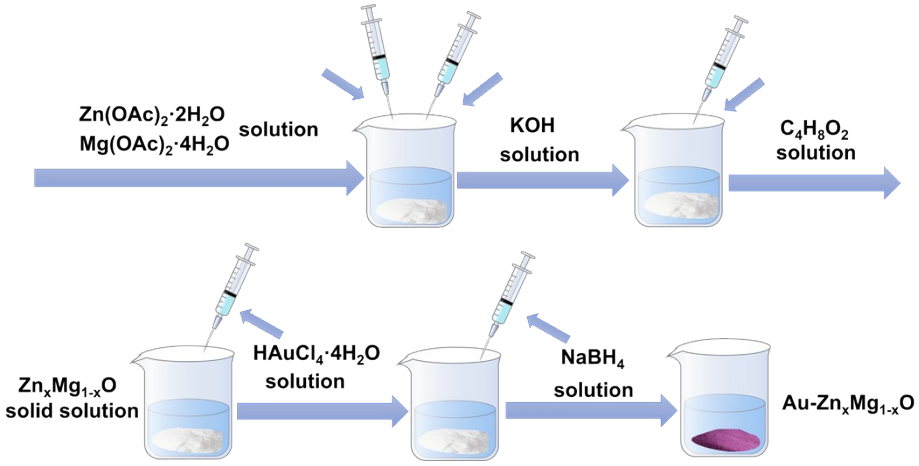

Fig. S1. Preparation method of $Zn_xMg_{1-x}O$ and Au-$Zn_XMg_{1-x}O$ sample.

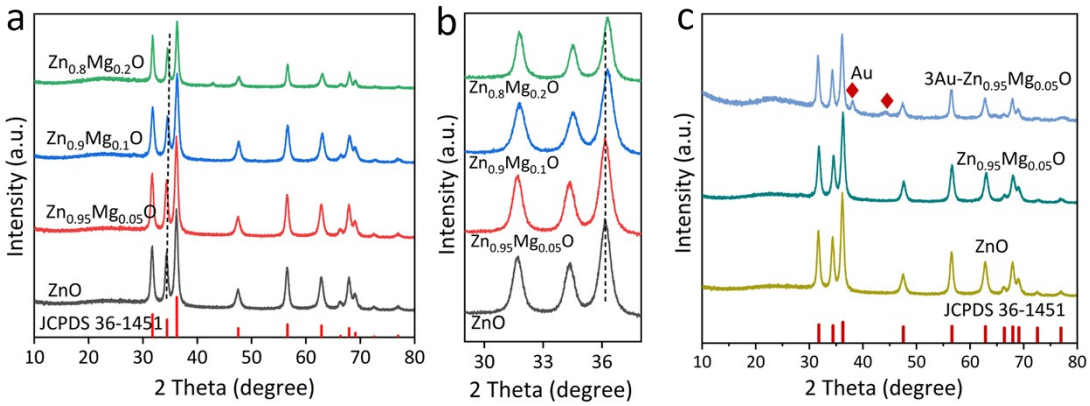

Fig. S2. (a) XRD patterns of the as-prepared different samples. (b) corresponding enlarged XRD patterns (31-32.5). (c) XRD patterns of ZnO, $Zn_{0.95}Mg_{0.05}O$ and 3Au-$Zn_{0.95}Mg_{0.05}O$ samples.

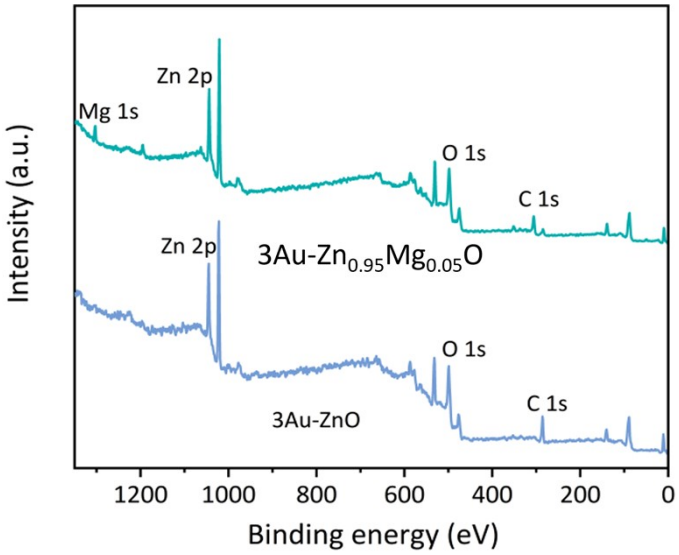

Fig. S3. The survey XPS spectra of 3Au-ZnO and 3Au-$Zn_{0.95}Mg_{0.05}O$ sample.

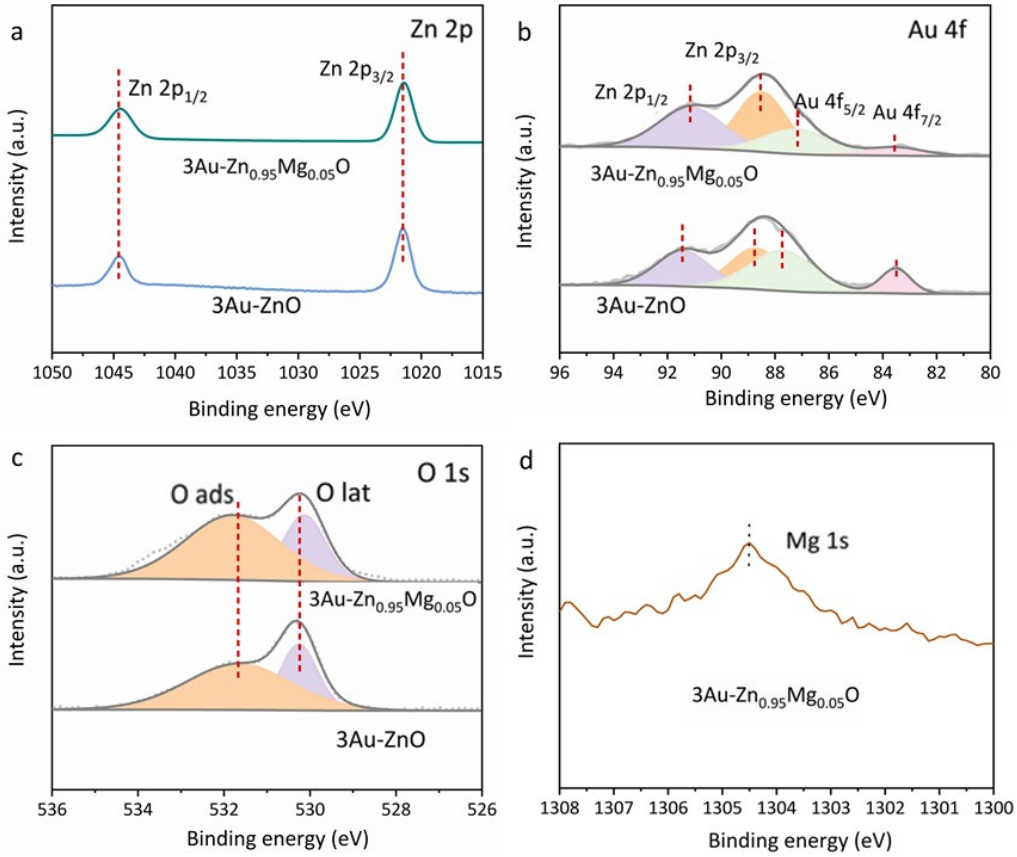

Fig. S4. High-resolution XPS spectra of 3Au-ZnO, 3Au-$Zn_{0.95}Mg_{0.05}O$ (a) Zn 2p (b) Au 4f, (c) O 1s, (d) Mg 1s.

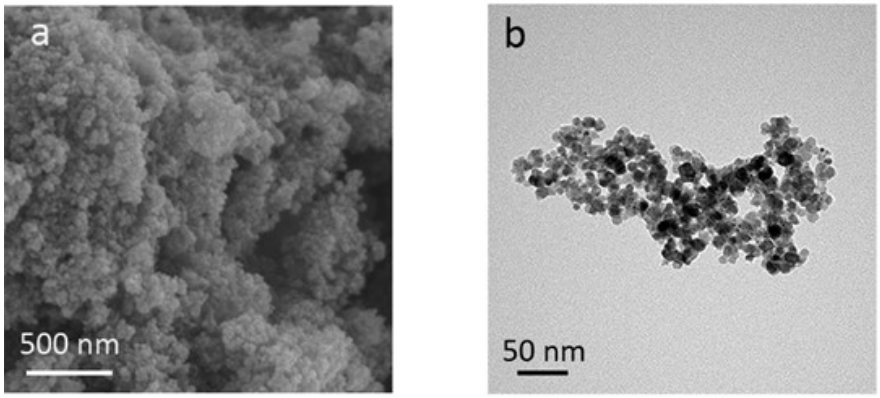

Fig. S5. (a) SEM image of $Zn_{0.95}Mg_{0.05}O$ sample. (b) TEM image of 3Au-$Zn_{0.95}Mg_{0.05}O$ photocatalyst.

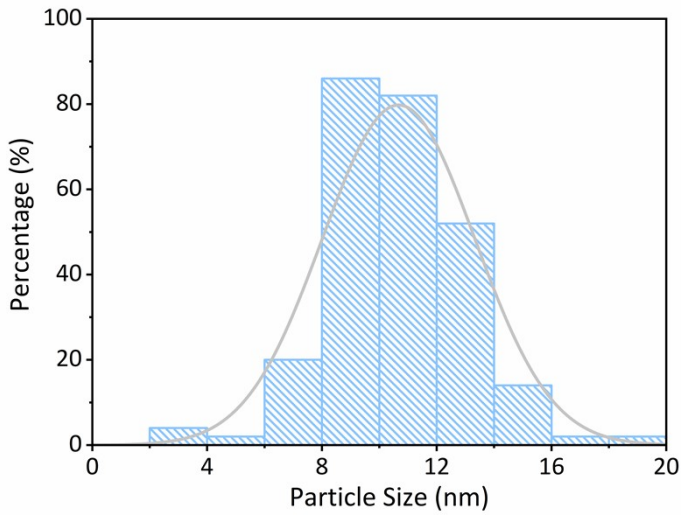

Fig. S6. Au nanoparticle size distribution of 3Au- $Zn_{0.95}Mg_{0.05}O$ sample.

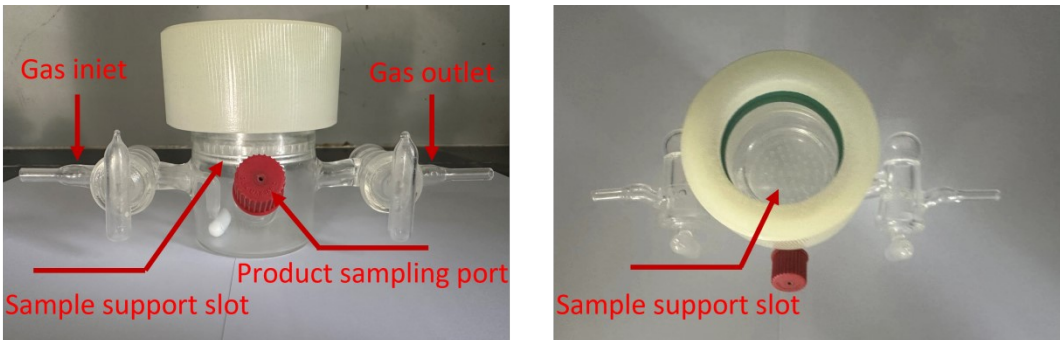

Fig. S7. Schematic illustration of the reactor for Photocatalytic Methane Oxidative Coupling.

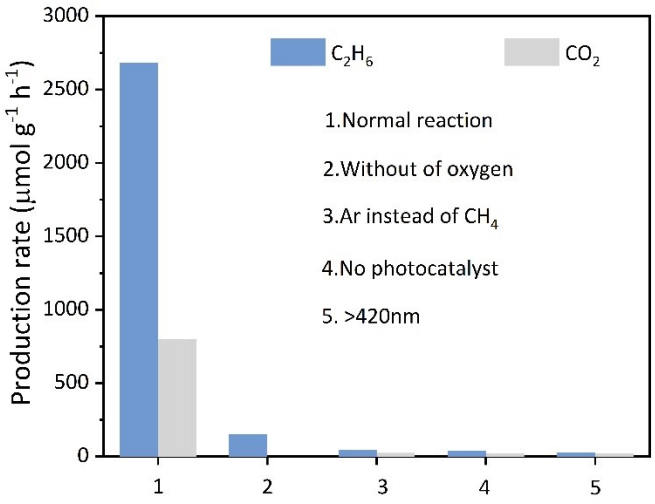

Fig. S8. Oxidative coupling performance of CH_4 under various conditions.

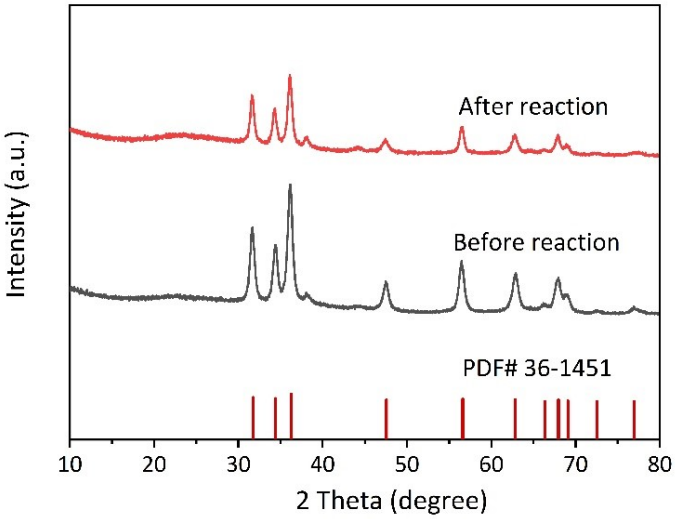

Fig. S9. XRD patterns of sample before and after the reaction.

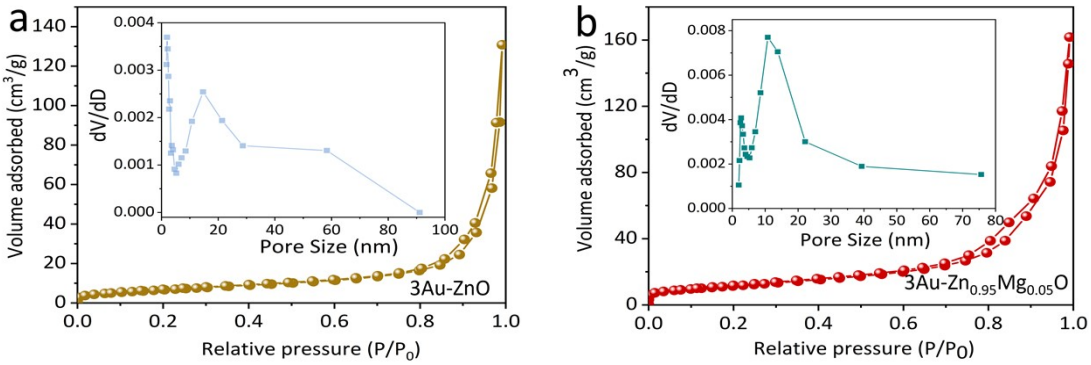

Fig. S10. 3Au-ZnO, and 3Au-$Zn_{0.95}Mg_{0.05}O$ sample: (a) N_2 adsorption-desorption isotherms. The inset is the corresponding pore-size distribution curve. (b) N_2 adsorption-desorption isotherms. The inset is the corresponding pore-size distribution curve.

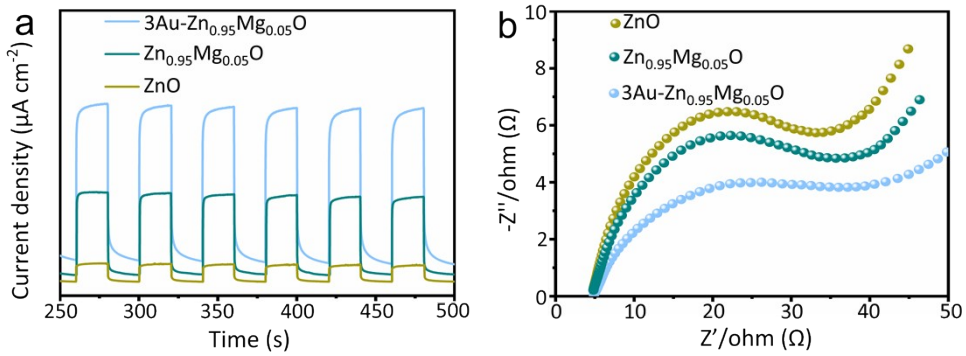

Fig. S11. ZnO, $Zn_{0.95}Mg_{0.05}O$ and 3Au-$Zn_{0.95}Mg_{0.05}O$ samples of (a) transient photocurrent generation, (b) EIS spectra.

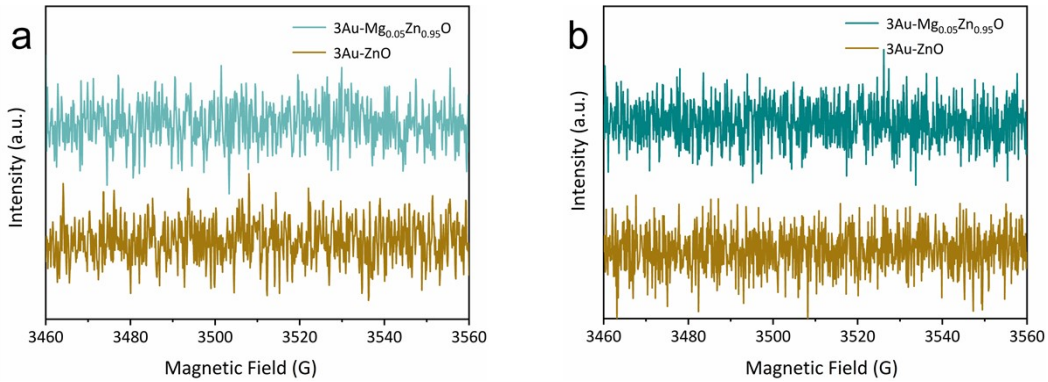

Fig. S12. (a) Detection of the methyl radical on 3Au-ZnO and 3Au-$Zn_{0.95}Mg_{0.05}O$. The EPR spectra are collected in CH_4 and H_2O at room temperature with DMPO as a trapping agent. (b) EPR spectra of spin-trapped radicals formed during dark of 3Au-ZnO and 3Au-$Zn_{0.95}Mg_{0.05}O$ dispersions saturated with air in methanol under dark.

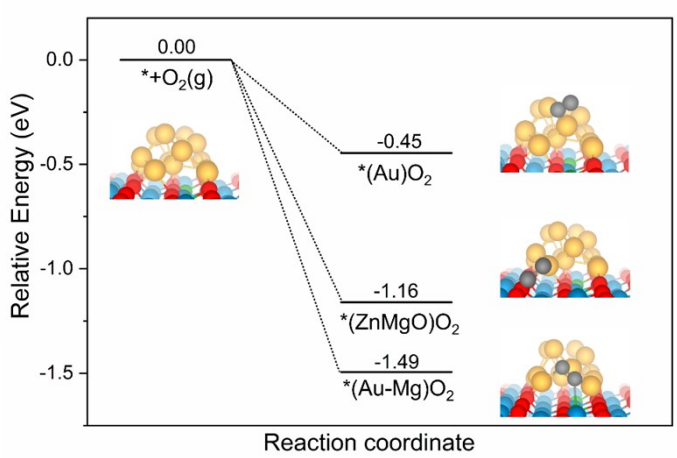

Fig. S13 Adsorption of O_2 on Au-ZnMgO surface. *(Au)O_2, *(ZnMgO)O_2 and (Au-Mg)O_2 represents three different adsorption configurations. O_2 adsorbed in a terminal manner on the Au surface, O_2 adsorbed on the ZnMgO substrate surface, and O_2 bridging between Au and Mg at the interface, respectively.

The adsorption energy of O_2 adsorbed on three different sites are -1.49, -1.16 and -0.45 eV. It is evident that the O_2 molecule is adsorbed strongly at the Au-ZnMgO interface with the O−O bond length of 1.41 Å, which is close to the typical value of peroxides (1.49 Å).[1] This suggests that photogenerated electrons injected into Au can easily dissociate this configuration of oxygen into *O. For O_2 adsorbed on Au, the O-O bond length is 1.28 Å, which is like the double bond length of O_2 (1.21 Å),[2] indicating a weaker adsorption. The adsorption on the ZnMgO substrate is even weaker, with an adsorption energy of -0.11 eV, significantly lower than the other two.

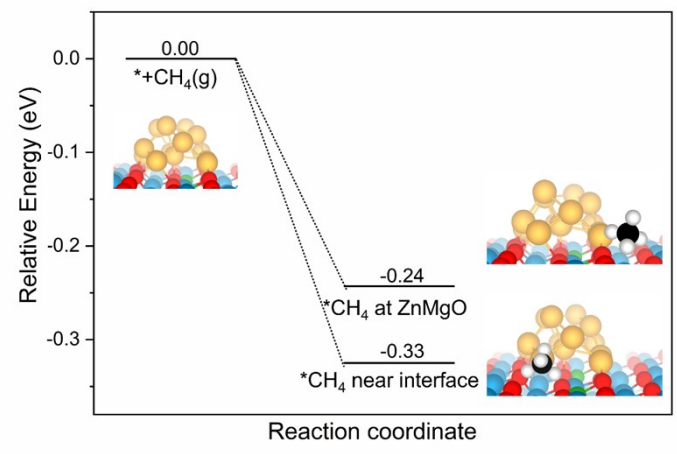

Fig. S14 The corresponding adsorption structural model of CH_4 on the surface of Au-ZnMgO.

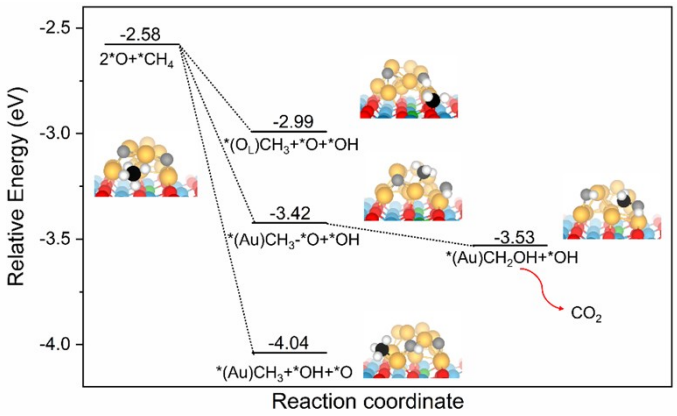

Fig. S15 Dissociation of $*CH_4$ on Au-ZnMgO surface. $*(O_L)CH_3$+*OH+*O, $*(Au)CH_3$-*O+*OH and $*(Au)CH_3$+*OH+*O represent three different configurations: CH_3 adsorbed on lattice oxygen (O_L) of substrate surface, $*CH_3$ adsorbed on the Au surface near *O, and $*CH_3$ bonded with Au and away from *O, respectively. Among these, when the methyl group is close to *O, it can easily form an over-oxidized intermediate $*CH_2OH$. After methane is dissociated by hole, the resulting methyl group readily adsorb onto the Au surface, while the *H is captured by *O, leading to form *OH.

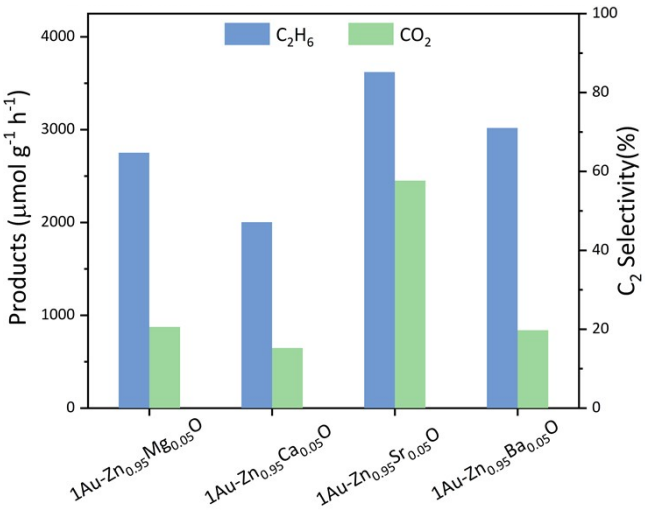

Fig. S16 Test results of different alkaline earth metals.

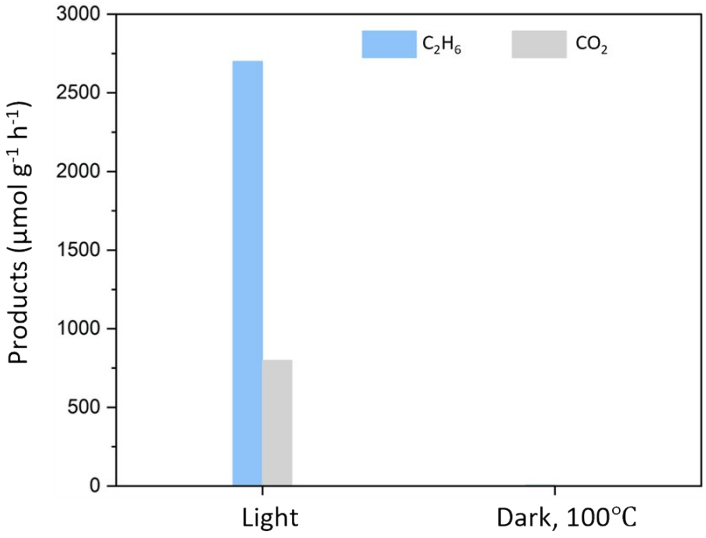

Fig. S17. Control experiments with different reaction conditions (3Au-$Zn_{0.95}Mg_{0.05}O$).

Table S1. Performance of different photocatalysts for photocatalytic reduction of CO_2.

Catalyst	Catalyst content	Products (μ mol g^{-1} h^{-1})	Selectivity (%)	Ref
Au-Bi_2WO_6	0.03 g, 365 W UV LED, glass reactor (3 oz, ca.88.7 mL in total volume), 20 bar total gas (CH_4 and O_2) with different ratios of CH_4 and O_2	1690	85	[S-4]
Au-$Zn_2Ti_3O_8$	0.03g, 365 nm LED, 1 atm, CH_4 and O_2, reactor	609.9	80.18	[S-5]
Au-ZnO	0.005 g,0.005g, 365 nm LED, CH_4/O_2 volume ratio = 99/1, 0.1 MPa, stainless-steel reaction chamber (volume 56 cm^3)	683	83	[S-6]
Au-$ZnGa_2O_4$	0.01 g, 150 mL quartz batch reactor, 4 mL of pure CH_4 gas and a certain volume of oxygen, 300 W xenon lamp	1315	53	[S-7]
6Wt% Ag HPW/TiO_2	0.1g, 400 W Xe lamp, stainless-steel batch reactor (volume ≈ 250 ml), CH_4, 0.3 MPa	20.6	90	[S-8]
Pt/TiO_2	0.075 g, UV lamps with a wave	55.6	61.7	[S-9]

	length centered at 254 nm, reaction system was remained at 25℃， 80 mL CH_4 + 75mL H_2O			
4.8 mol%Au/ZnO	0.001 g, 0.001 g, 300 W Xe lamp, 40 mL Schlenk flask reactor, pressure and ambient temperature, 1.0 bar of Ar was introduced with a syringe via the septum, and then 0.5 mL CH_4 gas was injected into the reactor.	11.4	95.9	[S-10]
Pd_1/TiO_2	0.003 g, 300 W Xe lamp, CH_4 atmosphere (0.1 MPa) at room temperature in a 30 mL custom-made quartz tube reactor.	913	94.3	[S-11]
Pt/HGTS	0.2 g, quartz reaction vessel (45 cm^3), 44.6 μmol of CH_4, 300 W Xe lamp	1.68	90	[S-12]
Au-$Zn_{0.95}Mg_{0.05}O$	0.005	2700	85	This work

Table S2. Control experimental results of the oxidative methane coupling over the 3Au-$Zn_{0.95}Mg_{0.05}O$ photocatalyst.

Catalyst	Reaction conditions	Products (μmol $g^{-1}h^{-1}$)
3Au-$Zn_{0.95}Mg_{0.05}O$	CH_4, solar light	C_2H_6 (2700), CO_2 (798)
3Au-$Zn_{0.95}Mg_{0.05}O$	>400nm	none
3Au-$Zn_{0.95}Mg_{0.05}O$	Ar instead of CH_4	none
3Au-$Zn_{0.95}Mg_{0.05}O$	no photocatalyst	none

Table S3. Surface area, pore diameter and pore volume for 3Au-ZnO, and 3Au-$Zn_{0.95}Mg_{0.05}O$.

Samples	BET surface area (m^2/g)	Pore volume (cm^3/g)	Pore diameters (nm)
3Au-ZnO	23.87	0.192	21.9
3Au-$Zn_{0.95}Mg_{0.05}O$	40.55	0.242	16.3

Reference:

[1] G. Kresse, J. Furthmüller. Efficient iterative schemes for ab initio total-energy calculations using a plane-wave basis set. Physical Review B, 54(1996): 11169-11186.

[2] J.P. Perdew, K. Burke, M. Ernzerhof. Generalized Gradient Approximation Made Simple. Physical Review Letters, 77(1996): 3865-3868.

[3] G. Kresse, D. Joubert. From ultrasoft pseudopotentials to the projector augmented-wave method. Physical Review B, 59(1999): 1758-1775.

[4] M. Fei, B. Williams, L. Wang, H. Li, Y. Yuan, J.R. Wilkes, T. Liu, Y. Mu, J. Huang, J. Nyakuchena, J. Huang, W. Li, D. Wang. Highly Selective Photocatalytic Methane Coupling by Au-Modified Bi_2WO_6. ACS Catalysis, 14(2024): 1855-1861.

[5] Q. Huang, J. Cai, F. Wei, Y. Fan, Z. Liang, K. Liu, X.F. Lu, Z. Ding, S. Wang. Selective oxidative coupling of methane to ethane with oxygen using an $Au/Zn_2Ti_3O_8$ photocatalyst under mild conditions. Journal of Materials Chemistry A, 12(2024): 21334-21340.

[6] P. Wang, R. Shi, Y. Zhao, Z. Li, J. Zhao, J. Zhao, G.I.N. Waterhouse, L.Z. Wu, T. Zhang. Selective Photocatalytic Oxidative Coupling of Methane via Regulating Methyl Intermediates over Metal/ZnO Nanoparticles. Angewandte Chemie International Edition, 62(2023).

[7] Y. Chai, S. Tang, Q. Wang, Q. Wu, J. Liang, L. Li. Gold nanoparticles supported on $ZnGa_2O_4$ nanosheets as efficient photocatalysts for selective oxidation of methane to ethane under ambient conditions. Applied Catalysis B: Environmental, 338(2023).

[8] X. Yu, V.L. Zholobenko, S. Moldovan, D. Hu, D. Wu, V.V. Ordomsky, A.Y. Khodakov. Stoichiometric methane conversion to ethane using photochemical looping at ambient temperature. Nature Energy, 5(2020): 511-519.

[9] L. Yu, Y. Shao, D. Li. Direct combination of hydrogen evolution from water and methane conversion in a photocatalytic system over Pt/TiO_2. Applied Catalysis B: Environmental, 204(2017): 216-223.

[10] L. Meng, Z. Chen, Z. Ma, S. He, Y. Hou, H.-H. Li, R. Yuan, X.-H. Huang, X. Wang, X. Wang, J. Long. Gold plasmon-induced photocatalytic dehydrogenative coupling of methane to ethane on polar oxide surfaces. Energy & Environmental Science, 11(2018): 294-298.

[11] W. Zhang, C. Fu, J. Low, D. Duan, J. Ma, W. Jiang, Y. Chen, H. Liu, Z. Qi, R. Long, Y. Yao, X. Li, H. Zhang, Z. Liu, J. Yang, Z. Zou, Y. Xiong. High-performance photocatalytic nonoxidative conversion of methane to ethane and hydrogen by heteroatoms-engineered TiO_2. Nature Communications, 13(2022).

[12] S. Wua, X. Tanc, J. Leia, H. Chenb, L. Wanga*, J. Zhanga*. Ga-doped and Pt-loaded Porous TiO_2-SiO_2 for Photocatalytic.pdf>. Journal of the American Chemical Society, 141(2019).